Task 3 Report: Literature Review of Spirals under Impact Loading and Bending

Evaluation of Glass Fiber Reinforced Polymer (GFRP) Spirals in Corrosion Resistant Concrete Piles

FDOT Contract Number: BDV30 977-27, FSU Project ID: 042924

Progress report date: 12/26/2019

(Initial submission to FDOT Structures Research Center: 9/23/2019; First revision: 11/5/2019)

Submitted to:

Florida Department of Transportation

Research Center

605 Suwannee Street

Tallahassee, Florida 32399-0450

Project Managers:

Christina Freeman	FDOT Structures Research Center
Ge Wan	FDOT Structures Design Office
Rodrigo Herrera	FDOT Structures Design Office

FAMU-FSU Engineering

Prepared by:

Olayiwola Adegbulugbe	Graduate Research Assistant
Sungmoon Jung	Principal Investigator
Raphael Kampmann	Co-Principal Investigator

Department of Civil and Environmental Engineering

FAMU-FSU College of Engineering

2525 Pottsdamer St., Tallahassee, FL. 32310.

Table of Contents

Chapter 1. Literature Review 1

1.1 Driving Stresses 1

1.2 Confinement in Concrete 2

1.2.1 Transverse Reinforcement Effects and Requirements 3

1.3 GFRP Stirrups/Spirals as Confinement during Pile Driving – Lesson Learned 9

1.4 Pile Driving Process Energy and Stresses 10

1.5 Strain Rate Effect on the Dynamic Properties of Fiber Reinforced Polymer 13

1.6 Finite Element Models for Concrete 16

1.7 Pile Test Instrumentation 18

1.7.1 Instrumentation for Impact Test 18

1.7.2 Instrumentation for Flexure Test 18

1.7.3 Instrumentation for Axial Test 19

1.7.4 Instrumentation Summary 19

Bibliography 20

LIST OF FIGURES

Figure 1.1: Confining action of spirals. 4
Figure 1.2: Schematic representation of the various energies involved in the process of driving a pile (So & Ng, 2010). 11
Figure 1.3: Wave equation model (Lee, Chow, Karunaratne, & Wong, 1988). 12
Figure 1.4: Comparison of the stress-strain curve for steel and FRPs. 15

LIST OF TABLES

Table 1.1: Typical tensile properties of reinforcement 14

Chapter 1. Literature Review

Confinement in precast piles are generally provided by spirals. In addition to restraining the lateral expansion of the concrete core, the spirals maintain the position of the longitudinal reinforcement under high loads, provide increased ductility, enhance the load carrying capacity of the pile, and sustain impact forces during pile driving. Spirals are designed such that the confining action they provide would compensate for load capacity losses resulting from concrete spalling. In Florida, piles are often installed in aggressive environments. Such exposure may result in the corrosion of steel reinforcement which could deteriorate piles and affect the long-term durability of the piles. The resistance of Fiber-reinforced polymer (FRP) spirals to corrosion makes them a good alternative to steel in concrete piles. The following review investigates the performance of spiral reinforcement in concrete piles, the behavior of spirals under impact loading, and the comparison between the expected performance of FRP spirals and conventional steel spirals especially under impact loading.

1.1 Driving Stresses

Prestressed concrete piles are designed and manufactured to withstand handling stresses, service loads, and driving stresses (ACI 543-12). Impact forces from a pile driving hammer are transmitted to a concrete pile as compressive waves travel down the pile. Once the wave hits the pile toe, it is reflected within the pile as either a compression wave, when a hard stratum is beneath the pile toe, or as a tension wave when a soft stratum is beneath the pile toe. The reflected wave travels to the pile top, where it is reflected again. Generally, pile driving results in the highest stresses the pile will experience. Dynamic compressive stresses induced by pile driving largely exceed the static compressive stresses induced by service loads (ACI 543-12). Therefore, a pile must have adequate structural strength to resist the driving stresses to avoid being damaged. Also, the minimum compressive strength, f_c' of a prestressed concrete pile should be at least 5000 psi or greater as necessary at the time of driving (ACI 543R-12; PCI bridge design manual, 2003). It should also be noted that most pile materials have higher dynamic strength than static strength (Crapps, 2004).

According to PCI bridge design manual (2003) and ACI 543R-12, allowable driving stresses for a pile must not be exceeded by stresses obtained from the pile's wave equation analysis. Per

AASHTO-LRFD Bridge Design (2012) recommendations the driving stress limits for a concrete pile are given by Equations (1.1) to (1.3)

$$s_{apc} = 0.85f_c' - f_{pe} \quad \textit{(1.1) AASHTO compression stress limit (ksi)}$$

$$S_{apt} = 0.095\sqrt{f_c'} + f_{pe} \quad \textit{(1.2) AASHTO tension stress limit (ksi)}$$

$$S_{apt} = f_{pe} \quad \textit{(1.3) AASHTO tension stress limit in severe environment (ksi)}$$

However, FDOT (2019) uses the following equations to determine the maximum allowable pile driving stresses.

$$s_{apc} = 0.7f_c' - 0.75f_{pe} \quad \textit{(1.4) FDOT Compression stress limit (psi)}$$

$$s_{apt} = 6.5(f_c')^{0.5} + 1.05f_{cpe} \quad \textit{(1.5) FDOT Tension stress limit for piles less than 50 ft. long (psi)}$$

$$s_{apt} = 3.25(f_c')^{0.5} + 1.05f_{cpe} \quad \textit{(1.6) FDOT Tension stress limit for piles 50 ft. and greater (psi)}$$

where f_{pe} is the effective prestressing stress in concrete (after all losses), f_{cpe} is the effective prestress (after all losses), taken as 0.8 times the initial prestress force divided by the minimum net concrete cross-sectional area of the pile, and f_c' is the compressive strength of concrete. Notations for the AASHTO equations are modified herein for easy comparison with the FDOT equations.

1.2 Confinement in Concrete

Concrete confinement by the transverse reinforcement has significant effects on the strength and ductility of concrete. The confining action of transverse reinforcement is activated by lateral pressure generated by the expansion of concrete under axial compression, at stresses close to the

unconfined strength of concrete. In addition to confining the concrete within the core of the pile, confinement reinforcement controls longitudinal cracks resulting from handling, driving or the design load. Longitudinal spacing between pile turns (spiral pitch) are more closely spaced at the pile head and pile toe for energy absorption and to resist splitting stresses that could result from pile driving activities.

1.2.1 Transverse Reinforcement Effects and Requirements

Compressive loads cause concrete to shorten longitudinally under uniaxial stress, and due to Poisson's effect and microcracking, the concrete also expands laterally. The lateral expansion of concrete within the spirals or core (out-to-out of spirals) is restrained by the spirals. This induces a lateral tensile stress on the spirals. Consequently, concrete within the core is also subjected to a lateral compressive stress. This implies that concrete element within the core is under triaxial compression, which increases the strength and ductility of concrete. Martinez, Nilson & Slate (1984) and Pantelides, Gibbons & Reavely (2013) stated that, for columns confined by steel spirals, the confined compressive strength of normal weight reinforced concrete, f'_{cc}, is given by Equation (1.7)

$$f'_{cc} = 0.85f'_c + 4.0f_l\left(1 - \frac{s}{d_c}\right) \qquad (1.7)$$

where f_l is the confining lateral compressive strength produce by the steel spiral, f'_c is unconfined concrete strength, and $\left(1 - \frac{s}{d_c}\right)$ represents the confinement effective stress factor, which shows that the confinement becomes less effective as the spiral pitch, s, increases and approaches the core diameter, d_c. It should be noted that $0.85f'_c$ in Equation (1.7) represents the in-place concrete strength.

Also, the confining lateral compressive strength as shown in Figure 1.1 produced by the steel spirals is given by Equation (1.8)

$$f_l = \frac{2A_{sp}f_{sp}}{sd_c} \qquad (1.8)$$

where A_{sp} is the cross-sectional area of the spiral and f_{sp} is the stress in the spiral at maximum load.

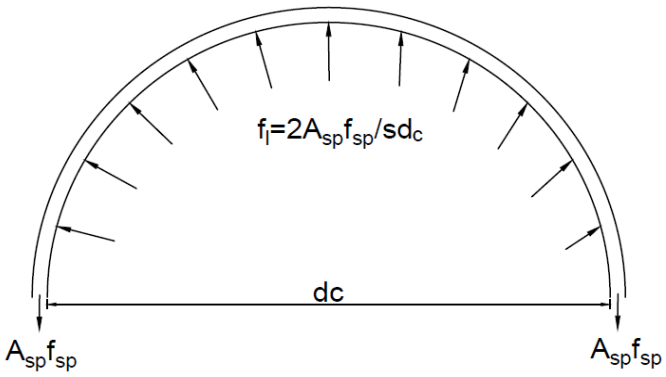

Figure 1.1: Confining action of spirals.

Mander, Priestley, & Park, (1988) provided a comprehensive model for the confined compressive strength of concrete reinforced with steel spirals as seen in Equation (1.9)

$$f'_{cc} = 0.85f'_c\left(-1.254 + 2.254\sqrt{1 + 7.94\frac{f'_l}{0.85f'_c}} - 2\frac{f'_l}{0.85f'_c}\right) \quad (1.9)$$

where the effective lateral confining compressive strength for steel spirals, f'_l is

$$f'_l = k_e\frac{2A_{sp}f_{yh}}{sd_c} \quad (1.10)$$

Afifi, Mohamed, & Benmokrane (2015) and Mousa, Mohamed, & Benmokrane (2018) stated the confined concrete strength for concrete reinforced with GFRP spirals as Equation (1.11) and Equation (1.12) respectively.

$$f'_{cc} = 0.85f'_c\left(1 + 4.547\left(\frac{f'_l}{0.85f'_c}\right)^{0.723}\right) \quad (1.11)$$

$$f'_{cc} = 0.85f'_c\left(0.85 + \sqrt{0.17 + 6.43\frac{f'_l}{0.85f'_c}} - 2\frac{f'_l}{0.85f'_c}\right) \quad (1.12)$$

where the effective lateral confining compressive strength for GFRP spirals, f'_l is

$$f_l' = k_e \frac{2A_{sp} f_{fb}}{s d_c} \quad (1.13)$$

and the confinement effectiveness coefficient, k_e is

$$k_e = \frac{1 - (s'/2d_c)}{1 - \rho_{cc}} \quad (1.14)$$

where A_{sp} is the cross-sectional area of GFRP spiral, s is the pitch of the spirals; s' is the clear spacing between spirals; d_c is the concrete core diameter from the spiral centerline; ρ_{cc} is the ratio of area of longitudinal reinforcement to area of core of section; and f_{fb} is the bend strength of spirals recommended in ACI 440.1R-15 (2015) as

$$f_{fb} = \left(0.05 \frac{r_b}{d_b} + 0.3\right) f_{fu} \leq f_{fu} \quad (1.15)$$

where r_b is the inner radius of the spirals; d_b is the diameter of the spiral bars; and f_{fu} is the ultimate tensile strength of the straight FRP bars.

Section 932-3.3.1 of the FDOT Standard Specifications for Road and Bridge Construction (2019) requires that the minimum strength of bent bars (90° bends), be no less than 60% of the straight bar strength.

The concept of the ACI specification on spiral reinforcement is that it should be sufficient to increase the capacity of the core by an amount equivalent to the capacity of the shell. This ensures that capacity is maintained if the shell spalls off. The transverse reinforcement ratio for pile reinforced with spirals according to ACI specifications (ACI 318-14; ACI 543R-12) is required to be

$$\rho_s = 0.45 \left(\frac{A_g}{A_c} - 1\right) \frac{f_c'}{f_{yh}} \quad (1.16)$$

or,

$$\rho_s = 0.12 \frac{f_c'}{f_{yh}} \quad (1.17)$$

whichever is greater

where ρ_s is the ratio of the volume of spiral reinforcement to the volume of concrete core (out-to-out of spiral), i.e. $4A_{sp}/sd_c$, A_g is the gross area of the pile, A_c is the area of pile core (out-to-out

of spiral), f_{yh} is the yield strength of spiral reinforcement, and f_c' is the specified compressive strength of concrete.

Equations (1.16) and (1.17) above were specifically derived for circular spirals. However, ACI 318 also provides more empirical equations for square or rectangular transverse reinforcement as follows:

$$A_{sh} = 0.3sh_c\left(\frac{A_g}{A_c} - 1\right)\frac{f_c'}{f_{yh}} \tag{1.18}$$

or,

$$A_{sh} = 0.09sh_c\frac{f_c'}{f_{yh}} \tag{1.19}$$

whichever is greater

where A_{sh} is the total cross-sectional area of transverse reinforcement in the direction considered, s is the spacing of tie sets in the longitudinal direction, and h_c is the width of the core in the direction considered.

For piles, the ACI spiral equations are not generally applicable therefore these equations were adjusted for piles in seismic regions. PCI recommendation for transverse reinforcement for prestressed concrete pile in regions of low to medium seismic risk is

$$\rho_s = 0.12\left(\frac{f_c'}{f_{yh}}\right) \geq 0.007 \tag{1.20}$$

where $f_c' \leq 6000$ psi (40 MPa) and $f_y \leq 85{,}000$ psi (585 MPa).

In regions of high seismic risks, the PCI recommendation for minimum amount of transverse reinforcement for prestressed concrete pile with circular ties or spirals is

$$\rho_s = 0.45\left(\frac{f_c'}{f_{yh}}\right)\left(\frac{A_g}{A_c} - 1\right)\left[0.5 + 1.4\frac{P_u}{f_c'A_g}\right] \tag{1.21}$$

but not less than

$$\rho_s = 0.12\left(\frac{f_c'}{f_{yh}}\right)\left[0.5 + 1.4\frac{P_u}{f_c'A_g}\right] \tag{1.22}$$

where P_u is the maximum factored axial compressive load on the pile, $f_c' \leq 6000$ psi (40 MPa) and f_y is the yield strength of transverse reinforcement $\leq 85{,}000$ psi (585 MPa).

In regions of high seismic risks, the PCI recommendation for total area of transverse reinforcement, A_{sh}, in the direction considered for prestressed concrete pile with square spirals or ties is:

$$A_{sh} = 0.3sh_c \frac{f_c'}{f_y}\left(\frac{A_g}{A_c} - 1\right)\left[0.5 + 1.4\frac{P_u}{f_c' A_g}\right] \quad (1.23)$$

but not less than

$$A_{sh} = 0.12sh_c \frac{f_c'}{f_y}\left[0.5 + 1.4\frac{P_u}{f_c' A_g}\right] \quad (1.24)$$

where h_c is the cross-sectional dimension of pile core measured center-to-center of spiral or tie reinforcement and $f_y \leq 70{,}000$ psi (480 MPa).

Mohamed, Afifi, & Benmokrane (2014) tested fourteen (14) full-scale circular column specimens under concentric axial load. Six (6) specimens each were reinforced with GFRP and another six (6) were reinforced with CFRP rebars. The other two (2) reference columns were plain and steel RC specimens. All specimens had diameter of 300 mm and measured 1500 mm in length. Test parameters were confinement configuration (spirals versus hoops), hoop lap length, volumetric ratio, and FRP reinforcement type (GFRP versus CFRP).

FRP Spiral reinforcements were designed according to clause 8.4.3.13 of the Canadian Standards Association (2012) code requirements. It stipulates that spiral reinforcement shall have a minimum diameter of 6 mm, distance between spiral turns shall not exceed 1/6 of the core diameter, clear spacing between successive spiral turns shall not be less than 25 mm or exceed 75 mm, and the minimum volumetric ratio of spirals is given by

$$\rho_{Fs} = \frac{f_c'}{f_{Fh}}\left(\frac{A_g}{A_c} - 1\right)\left(\frac{P}{P_o}\right) \quad (1.25)$$

where

$$\left(\frac{P}{P_o}\right) \geq 0.2 \quad (1.26)$$

$$\left(\frac{A_g}{A_c}\right) \geq 0.3 \qquad (1.27)$$

where f_c' is the specified concrete compressive strength; f_{Fh} is the least of $\phi_{FRP} f_{fu}$, or the stress equivalent to a strain of $0.006E_f$ in the FRP, or the stress corresponding to the local failure of corners, hooks, bends, and laps; ϕ_{FRP} is the resistance factor for FRP reinforcement; P is the applied concentrated load which is assumed to be 0.65 times the nominal axial load capacity of the designed column, P_o. According to PCI Design Handbook (1999), for a prestressed concrete compression member P_o is given by:

$$P_o = \left(0.85f_c' - 0.6f_{pe}\right)A_g \qquad (1.28)$$

However, based on service loads, the allowable axial capacity N for prestressed concrete piles fully supported laterally by soil and primarily subjected to axial load is

$$N = \left(0.33f_c' - 0.27f_{pe}\right)A_g \qquad (1.29)$$

A factor of safety, P_o/N, between 2.0 and 3.0 is usually sufficient for short column piles (PCI Design Handbook, 1999).

FDOT Specifications 455-5.12 provides a more conservative equation that is in conformance with Equation (1.28).

FDOT Structures Design Guidelines (2018) require that the maximum driving resistance of a 24-inch pile must not exceed 450 tons (900 kip) unless justifiable reasons for exceeding this value is provided. This pile driving resistance corresponds to the required nominal bearing resistance of the pile. It should be noted that the maximum pile driving resistance does not represent a default value for design as subsoil conditions may require using a lesser value. The maximum driving resistance requirements for piles of other dimensions can be obtained from Table 3.5.12-1 of the FDOT Structures Design Guidelines.

According to Mohamed et al. (2014), the ratio f_{cc}'/f_{co}' , where f_{cc}' is the confined concrete strength and f_{co}' is the in-place compressive strength of the unconfined concrete in the column ($0.85f_c'$) indicates the strength enhancement of the concrete core by the confining FRP spirals and hoops. The ratio of f_{cc}'/f_{co}' obtained for the FRP RC columns ranged from 1.38 to 1.81, and ductility

ranged from 1.63 to 2.53. This shows the ductility enhancement capabilities of the confining FRP reinforcements even when the concrete cover has spalled.

Other requirements for confinement reinforcement in terms of the cross-sectional area, pitch and turns according to PCI are given below. It should be noted that these are minimum requirements and are applicable to cases where much of the length of the pile is supported laterally by soil and where minimum lateral loads act on the pile. The requirements are:

- For piles with nominal sizes equal to or less than 24 in., minimum spiral cross-sectional area, A_{sp}, is 0.034 in^2. Spiral pitch at both ends of the pile are 1 in. for 5 turns, followed by a pitch of 3 in. for 16 turns, and then a spiral pitch of 6 in. for the remaining portion along the pile length.
- For piles with nominal sizes greater than 24 in., minimum spiral cross-sectional area, A_{sp}, is 0.04 in^2. Spiral pitch at both ends of the pile are 1.5 in. for 4 turns, followed by a pitch of 2 in. for 16 turns, and then a spiral pitch of 4 in. for the remaining portion along the pile length.

FDOT Index 455-012 to 455-030 conforms with the PCI requirements for confinement reinforcement in terms of the cross-sectional area, pitch and number turns.

However, Benmokrane, Mohamed, ElSafty, & Nolan (2018) designed No. 5 GFRP spirals to provide confinement for the concrete core of 60-ft.-long 24-in. square concrete piles. Spiral pitch at both ends of the piles were 2 in. for 5 turns, followed by 3 in. for 16 turns, and then a spiral pitch of 6 in. for the remaining portion of the pile length.

1.3 GFRP Stirrups/Spirals as Confinement during Pile Driving – Lesson Learned

Vicaria, Diaz, Arroyo, & Paulotto (2014) analyzed results from the driving and high-strain dynamic tests performed on 400 mm (15.7 in.) square GRFP reinforced piles. The piles had a length of 12 m (39.3 ft.) and were reinforced longitudinally by 12 GFRP bars (3 at each corner). Each longitudinal reinforcement had a diameter of 20 mm. The piles were reinforced transversely by 10 mm GFRP stirrups. The authors reported an average crack width of 0.30 mm (0.01 in.) during the handling of the GFRP reinforced piles. These cracks were attributed to the lower axial

stiffness of the GFRP bars. The piles were driven to refusal using a hammer with a ram weight of 9 t and a constant drop height of 0.40 m. The drop height was increased to 1.20 m for the dynamic load tests. The authors stated that although large tensile stresses (> 15 MPa) were developed in the GFRP piles during pile driving, no damage resulted from the dynamic testing of the piles.

Benmokrane, Mohamed, ElSafty, & Nolan (2018) performed field test on two 60-ft.-long 24-inch square piles that were reinforced longitudinally by GFRP bars and transversely by GFRP spirals. For Pile 1, 20 No. 8 GFRP bars were used as longitudinal reinforcement. For Pile 2, 12 No. 8 GFRP bars were used as longitudinal reinforcement. In both piles No. 5 GFRP spiral reinforcement was used in the transverse direction. Reinforcement ratio for Pile 1 and 2 were 2.7 % and 1.6 % respectively. Spiral pitch at both ends of the piles are 2 in. for 5 turns, followed by a pitch of 3 in. for 16 turns, and then a spiral pitch of 6 in. for the remaining portion along the pile length. With no prestressing involved, the maximum allowed pile compressive stress was estimated as the first term of Equation (1.4), that is $0.7f_c'$. Although the piles were 60 ft. long, the maximum tensile stress was estimated by the first term of Equation (1.5), that is $6.5(f_c')^{0.5}$. Results from the test showed that the maximum compressive stresses measured in Pile 1 were within the allowable limit of 5.95 ksi, while the tensile stresses for a few end-of-drive blows were higher than the allowable limit of 0.6 ksi. The maximum compressive stresses measured in Pile 2 were also within the allowable limit of 5.95 ksi, while the tensile stresses at the end-of-drive were higher than the allowable limit of 0.6 ksi with values up to 1.6 ksi. Conclusively, the test showed that the concrete core of the piles was successfully confined by GFRP spirals with no cover spalling. Also, no cracks were observed, and no major pile damage resulted from compression loading.

1.4 Pile Driving Process Energy and Stresses

The drivability of a pile depends on the energy transferred to the pile by the hammer, the resistance offered by the soil, pile strength against driving stresses and the capability of the pile to transfer driving stresses from the pile top to the pile toe. The potential energy of a hammer falling under gravity is progressively converted into kinetic energy. On impacting the pile head (usually with a cushion), some energy is lost. The impact force at the top of the pile is assumed to make the pile behave like an elastic bar. Impact force delivered at the pile head travels longitudinally down the pile as a stress wave at a velocity dependent on the elastic modulus of the pile. As the stress wave

travels down the pile, some energy radiates into the soil along the shaft and at the pile toe. With enough driving force, the pile is advanced into the underlying soil.

Prior to analyzing piles based on wave equation, the dynamic equation using energies summarized in Figure 1.2 was used.

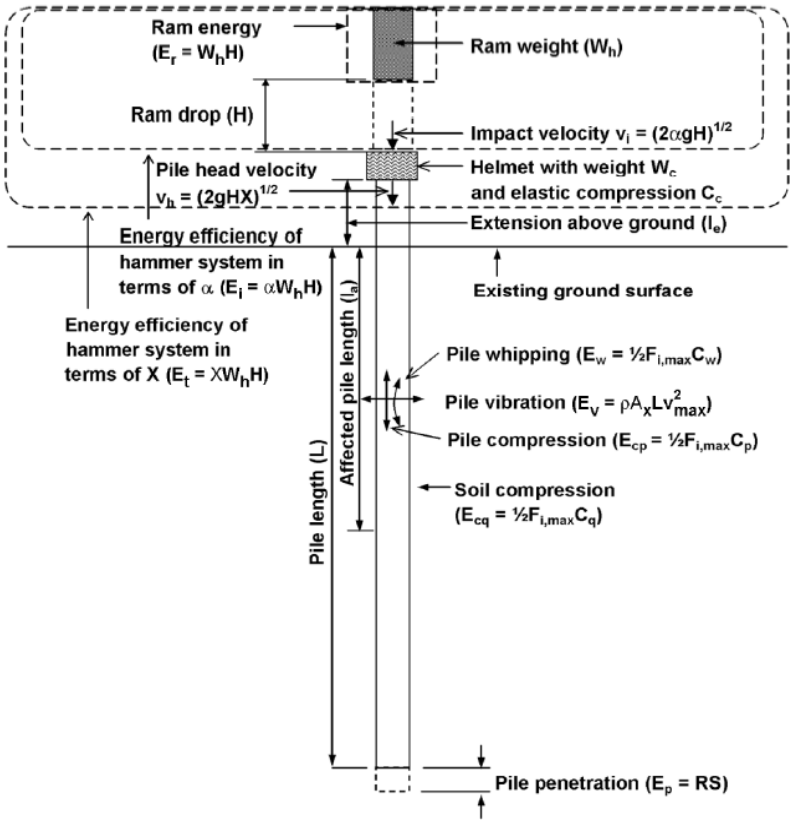

Figure 1.2: Schematic representation of the various energies involved in the process of driving a pile (So & Ng, 2010).

Equation (1.30) represents the pile driving process using the principle of energy balance.

$$E_t = E_c + E_v + E_{pen} \qquad (1.30)$$

where E_t is the transferred energy to the pile head, E_c is the strained energy stored in the pile and soil temporarily, E_v is the energy lost to pile vibration, and E_{pen} is the energy used to penetrate the soil.

The performance of the hammer is a measure of the transferred energy. Due to energy losses the transferred energy is smaller than the kinetic hammer energy.

In Figure 1.2 it is assumed that R is the force acting at the bottom of the pile. However, this assumption does not consider the skin friction resistance and the end bearing resistance, both of which changes during pile movement (Rajapakse, 2008). The dynamic equation (W_hH= RS) does not consider the stress distribution in the pile, the pile diameter or the pile type. It also considers the pile to be rigid, whereas the pile recoils and rebounds during driving. Smith (1960) devised a pile driving analysis model which analyzes pile driving as a problem involving longitudinal wave transmission. This analysis termed the wave equation analysis involves dividing the pile into small segments interconnected by pile springs. Side friction acting on each segment and the pile toe are also represented by several springs and dash pots Figure 1.3).

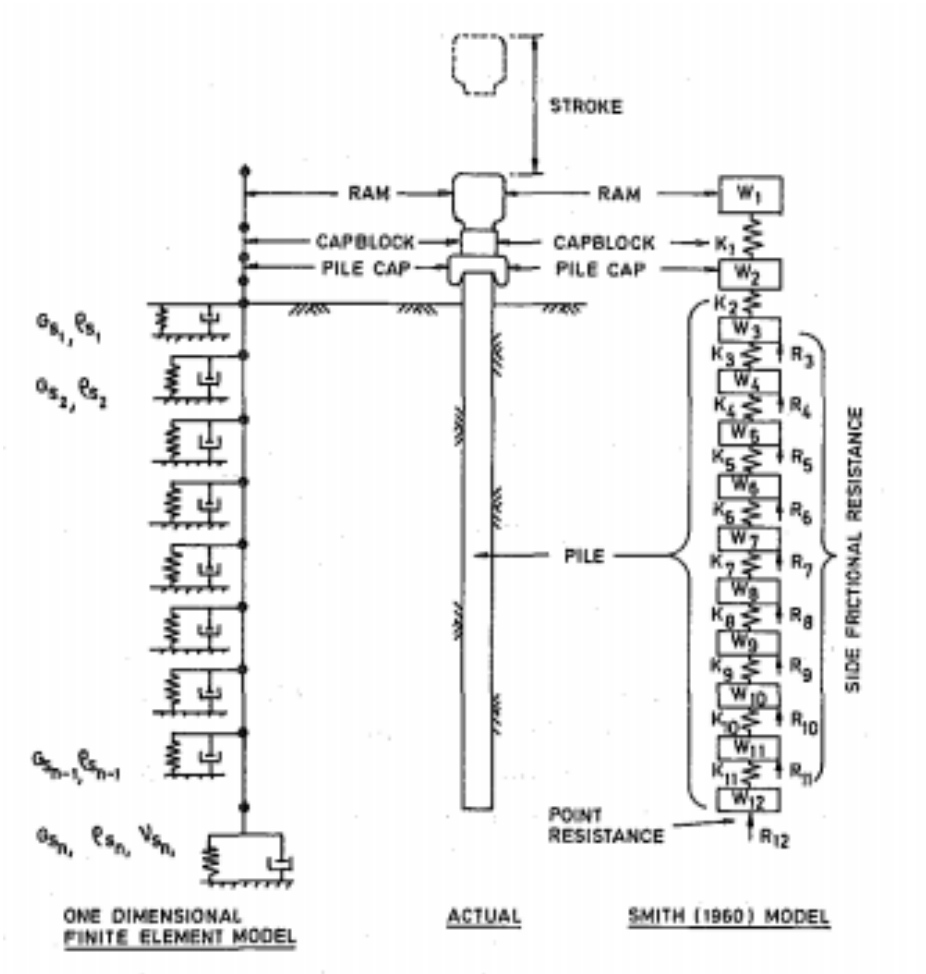

Figure 1.3: Wave equation model (Lee, Chow, Karunaratne, & Wong, 1988).

A pile is treated as an elastic bar along which only axial stress waves travel in analyzing the dynamic response of the pile to driving. The one-dimensional wave analysis of waves travelling up and down the pile can reflect the behavior of the pile. The axial wave velocity, c, of the travelling waves is given by:

$$c = \sqrt{E/\rho} \qquad (1.31)$$

where E is the modulus of elasticity and ρ is mass density of the pile material.

In addition to changes in the interaction of the pile with its immediate surroundings (i.e., materials at the pile top, along the shaft, and at the toe), changes in pile cross section determines the complexity and the number of waves travelling along the pile (Holeyman, 1992).

1.5 Strain Rate Effect on the Dynamic Properties of Fiber Reinforced Polymer

Fiber Reinforced Polymers (FRPs) are composed of fibers embedded in a polymeric resin matrix. FRP types include Aramid Fiber Reinforced Polymer (AFRP), Basalt Fiber Reinforced Polymer (BFRP), Carbon Fiber Reinforced Polymer (CFRP) and Glass Fiber Reinforced Polymer (GFRP). FRP reinforcement provides a corrosion resistant alternative to steel. The electromagnetic transparency (for GFRP), the high stiffness-to-weight and high strength-to-weight ratios of FRP reinforcement when compared to steel also make them desirable in concrete structures (Correia, Branco, & Ferreira, 2007; Robert & Benmokrane, 2013). While the fibers in an FRP reinforcement bears a significant portion of the applied load, the polymeric resin matrix ensures stress transfer among the fibers (Cantwell & Morton, 1991). FRPs are characterized by anisotropy and a linear elastic behavior till failure whereas steel is isotropic and yields significantly before failure. The typical tensile properties of reinforcement made from AFRP, BFRP, CFRP, GFRP and steel are summarized in Table 1.1. Figure 1.4 shows that steel exhibits greater ductility compared to the FRPs.

Table 1.1: Typical tensile properties of reinforcement

	AFRP	**BFRP**	**CFRP**	**GRFP**	**Steel**
Nominal yield stress, ksi (MPa)	NA	NA	NA	NA	40 – 75 (276 – 517)
Tensile strength, ksi (MPa)	250 – 386 (1720 – 2540)	150 – 240 (1035 – 1650)	87 – 535 (600 – 3690)	70 – 230 (483 – 1600)	70 – 100 (483 – 690)
Elastic Modulus, ksi (GPa)	6000 – 18200 (41 – 125)	6500 – 8500 (45 – 59)	15900 – 84000 (120 – 580)	5100 – 8700 (35 – 60)	29000 (200)
Yield strain, percent	NA	NA	NA	NA	0.14 – 0.25
Rupture strain, percent	1.9 – 4.4	1.6 – 3.0	0.5 – 1.7	1.2 – 3.1	6 – 12

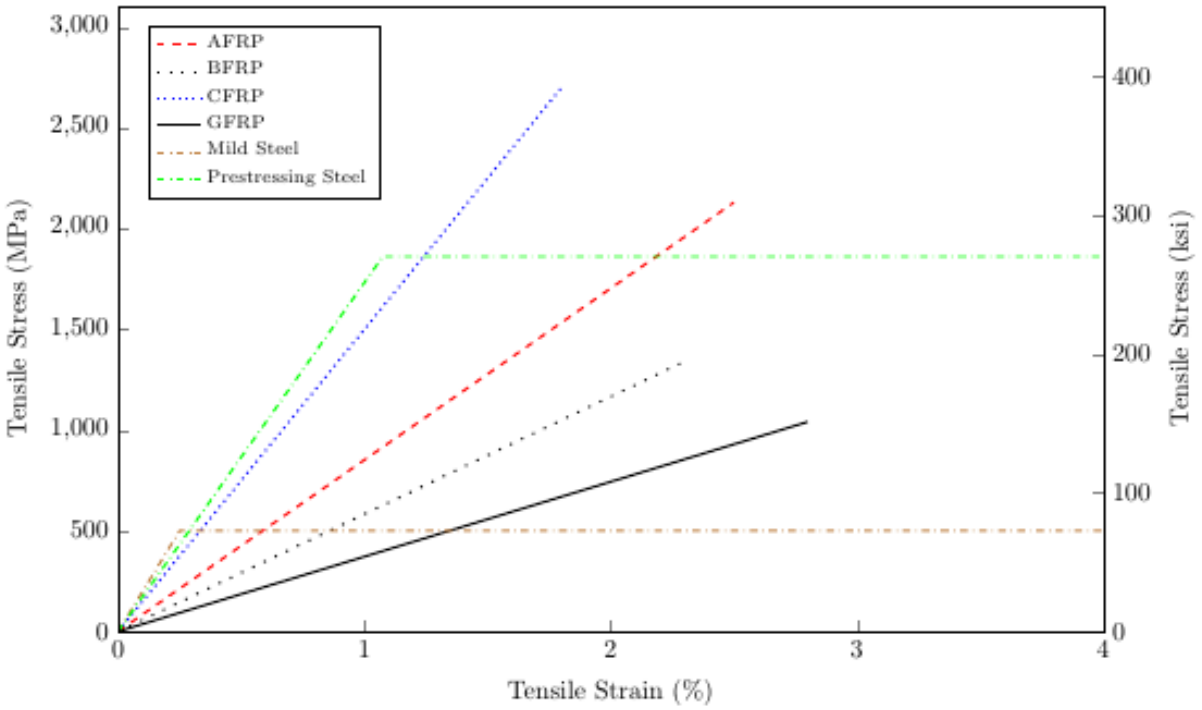

Figure 1.4: Comparison of the stress-strain curve for steel and FRPs.

Dynamic applications of FRP make it necessary to understand their mechanical properties under dynamic loads (or high strain rates). Impact is characterized by the application of a high intensity load rate within a short period. Several authors have investigated the effect of strain rates on the tensile, shear, compressive, and flexural properties of FRPs. Griffiths & Martin (1974) investigated the compressive dynamic properties of unidirectional CFRP at high strain rates. No strain rate effects were observed for changes in strain rate between 320 and 550 s^{-1}.

The tensile compressive mechanical properties of unidirectional glass/epoxy composites were studied under quasi-static and dynamic loading at various strain rates from 0.001 s^{-1} to 100 s^{-1} (Shokrieh & Omidi, 2009a, 2009b). Results showed a 52% and 53% increase in the modulus of elasticity and tensile strength with respect to the static value for the strain rate range described. Compressive strength and compressive modulus also increased by 66.9% and 53.4% respectively.

GFRP were tested under both quasi-static and dynamic tensile loadings to investigate the strain rate effect at five strain rates (1/600, 40, 80, 120 and 160 s^{-1}) by Ou & Zhu (2015). An increase in modulus of elasticity was reported over strain range of 40 s^{-1} to 160 s^{-1}. Tensile strength of GFRP

also increased. Several other authors have also reported longitudinal and transverse strength increase for GFRP under strain rate changes (Takeda & Wan, 1995; Tzeng & Abrahamian, 1996).

Ochola, Marcus, Nurick, & Franz (2004) studied the mechanical behavior of glass and carbon fiber reinforced composites at strain rates of 10^{-3} s^{-1} and 450 s^{-1}. Their results suggested that impact resistance of CFRP and GFRP under compression loading decreases with an increase in strain rate. In terms of ultimate compressive stress however, an increase of 20.9% occurred for GFRP compared to an increase of 0.6% for CFRP. This suggests that CFRP is strain rate insensitive under compressive dynamic loads. Also, an increase in modulus of elasticity was observed for both CFRP and GFRP at 73.9 % and 75.8% respectively.

Naresh, Shankar, Rao, & Velmurugan (2016) characterized the material behavior of glass/epoxy (GFRP) and carbon/epoxy (CFRP) composites at strain rates ranging from 0.0016 s^{-1} to 542 s^{-1}. They concluded that the tensile strength for GFRP increased by 66.3% compared to a 6.3% increase for CFRP. Also, modulus for GFRP went up 3.8 times its quasi-static value compared to 1.3 times for the CFRP.

Overall existing literature suggests that GFRP are strain rate sensitive to longitudinal compressive and tensile dynamic loads or high velocity impact, whereas CFRP have a weak dependence on strain rate. However, Melin & Asp (1999) also observed a weak dependency of the transverse tensile properties of CFRP on strain rate. Daniel, Hsiao, & Cordes (1995), also stated that for test conducted at rate ranges between 0.0001 s^{-1} and 500 s^{-1}, for CFRP, the longitudinal tensile and compression modulus increased with increasing strain rate; longitudinal tensile and compression strength were insensitive to rate changes; transverse tensile and compression modulus and strength increased with increasing strain rate.

Typical strain rate for pile driving is between 10^{-2} s^{-1} to 10 s^{-1} (Ortlepp & Curbach, 2004). Given that under dynamic conditions, the strain rate dependence of a material may be different from what is observed under quasi-static conditions, as observed in concrete, steel, and GFRP as discussed previously. These materials will be modeled as strain rate sensitive for finite element analysis.

1.6 Finite Element Models for Concrete

High velocity impacts and high strain rate behavior of materials are generally analyzed using an explicit solver such as the LS-DYNA software. Chen, Hao, & Chen (2015) investigated the

response of a prestressed reinforced concrete member to blast loading using LS-DYNA. To model the concrete the authors used the 8-nodes constant stress solid element (SOLID_164) with 1-point quadrature integration. Steel reinforcement was modelled using the 3-nodes beam element (BEAM_161) with 2 × 2 Gauss quadrature integration. *Contact Automatic Single Surface was defined to properly model the interface between the concrete and the reinforcement. To model concrete behavior, the material model *Mat Concrete Damage Rel3 (MAT_72_REL3) was used. The material model considers strain-rate effect, plasticity and damage softening after failure. *Mat Piecewise Linear Plasticity (MAT_024) was used to model the longitudinal and transverse reinforcements. *Mat Add Erosion was used to prevent computation overflow that could result from large deformation of concrete. The authors applied prestressing in the numerical model by applying initial hogging deformation to the member. The initial prestress was obtained by implicit analysis through ANSYS. This was then used as the initial condition for explicit analysis that followed in LS-DYNA.

Jiang & Chorzepa (2015) performed a failure analysis on prestressed concrete members subjected to lateral impact loads using LS-DYNA. For a prestressed concrete member models, the prestressing force should be applied before impact. The authors stated that prestressing force should be applied to the member by a temperature induce shrinkage because LS-DYNA cannot apply the prestressing force to the member directly. As cited by the authors, beam element representing the prestressing strands can be constrained to the concrete elements by using *Constrained Lagrange in Solid.

Wu, Crawford, & Magallanes (2012) analyzed three concrete models for quasi-static, blast and impact load analyses. These models are; *Mat Concrete Damage (MAT072), *Mat Winfrith Concrete (MAT078) and *Mat CSCM Concrete (MAT159). These models have relatively simple keyword inputs. The authors concluded that MAT072R3 modelled key concrete attributes such as post-peak softening, confinement dilation, strain rate effects and shear dilation satisfactorily. The model is therefore suitable for quasi-static, blast and impact load analyses. However, there were a few issues with the other two models (MAT078 and MAT159) as suggested by the authors.

Mutalib & Hao (2011) used the *Mat Concrete Damage Rel3 (MAT_72_REL3) model in LS-DYNA. Longitudinal and transverse reinforcements were modelled using the material model *Mat Piecewise Linear Plasticity. With this model an arbitrary stress-strain curve and strain rate

dependency of the reinforcement can be defined. Almusallam, Elsanadedy, Al-Salloum, & Alsayed (2013) also used the *Mat Piecewise Linear Plasticity to model the behavior of FRP rebars.

1.7 Pile Test Instrumentation

This section discusses the various instrumentation needed for the planned tests. Test piles will predominantly be tested under impact; however, flexure test and axial test will be carried out on one or two piles.

1.7.1 Instrumentation for Impact Test

Axial stress induced by the impactor should be measured by a pair of accelerometers and strain transducers installed externally on the sides of the pile close to the pile toe and/or the pile top. Data acquired from these transducers are transferred via a cable to the PDA. The PDA processes data from the accelerometer and strain gages to display a force and velocity versus time plot. According to ASTM D4945-17, the transducers should be located at a distance of at least 1.5 times the width of the pile from the pile toe and/or the pile top. The location of the transducers is such that irregular stress concentrations at the ends of the pile can be avoided during data collection. Strain changes in the spirals should also be monitored by strain gages attached to the spirals at several points along the pile length.

1.7.2 Instrumentation for Flexure Test

Measurements of the applied load, concrete strain, end slip, and deflections can be taken during the flexure test. Load is applied by an actuator and a spreader using four-point bending. To measure compressive strain at the top fiber, a pair of strain gages – with a center to center spacing of 1 ft. between them – should be located on the concrete surface at mid span. Two more strain gages should be placed equidistant on both sides of the midspan strain gages. Also, concrete strains on the sides of the pile should be measured by strain gages located on the concrete surface of both sides of the pile. Strand slip should be measured at the pile ends using end slip gages. Deflection measurements should be taken at several points along the pile using laser deflection gages. The instrumentation for flexure described here follows similar instrumentation by Roddenberry et al., 2014.

1.7.3 Instrumentation for Axial Test

Longitudinal strain measurements when the pile is under a concentric axial load can be measured using strain gages placed axially within the concrete core. The gages should be placed along the four sides of the pile within the concrete core. The gages should be placed at multiple levels within the pile (Fam et al., 2003;Pando, Filz, Ealy, & Hoppe, 2003). Transverse strains should also be measured by strain gages attached to the stirrups transversely. The same pile will be used for the flexural and axial tests. After the flexural test, the pile will be cut 6 ft. from both ends. Therefore, prior to casting, the pile should be instrumented such that two specimens for axial test can be obtained.

1.7.4 Instrumentation Summary

Given that the primary aim of this research is to investigate the performance of GFRP spirals under impact loading, the spirals will be adequately instrumented at critical locations along the pile length in addition to the instrumentation strategies utilized by the afore mentioned authors.

The goal of this task is to conduct relevant literature review, not the development of the final testing plan and instrumentation plan. Test plan and instrumentation drawings and instructions will be delivered in Task 4.

Bibliography

AASHTO-LRFD Bridge Design, S. (2012). American Association of State Highway and Transportation Officials. *Washington, DC*.

ACI Committee 318-14. (2014). *Building Code Requirements for Structural Concrete*. American Concrete Institute Farmington Hills, MI.

ACI Committee 440. (2015). *Guide for the Design and Construction of structural concrete reinforced with Fiber Reinforced Polymer (FRP) bars (ACI 440.1 R-15)*. American Concrete Institute Farmington Hills, MI.

ACI Committee 543-12. (2012). *Guide To Design, Manufacture, and Installation of Concrete Piles*. American Concrete Institute Farmington Hills, MI.

Afifi, M. Z., Mohamed, H. M., & Benmokrane, B. (2015). Theoretical stress-strain model for circular concrete columns confined by GFRP spirals and hoops. *Engineering Structures*.

Almusallam, T. H., Elsanadedy, H. M., Al-Salloum, Y. A., & Alsayed, S. H. (2013). Experimental and numerical investigation for the flexural strengthening of RC beams using near-surface mounted steel or GFRP bars. *Construction and Building Materials*.

ASTM D4945-17. (2017). Standard Test Method for High-Strain Dynamic Testing of Deep Foundations. *American Society for Testing and Materials*.

Benmokrane, B., Mohamed, H. M., ElSafty, A., & Nolan, S. (2018). *Field Driving Tests of Precast Concrete Piles Reinforced with GFRP Bars and Spirals*.

Canadian Standards Association. (2012). Design and Construction of Building Structures with Fibre-Reinforced Polymers,(CAN/CSA S806-12). *Canadian Standards Association Mississauga, Ont*.

Cantwell, W. J., & Morton, J. (1991). The impact resistance of composite materials - a review. *Composites*.

Chen, W., Hao, H., & Chen, S. (2015). Numerical analysis of prestressed reinforced concrete beam subjected to blast loading. *Materials and Design*.

Comm Rep. (1974). Recommendations for Design, Manufacture, and Installation of Concrete Piles. *J Am Concr Inst*, *71*(10), 477–492.

Correia, J. R., Branco, F. A., & Ferreira, J. G. (2007). Flexural behaviour of GFRP-concrete hybrid beams with interconnection slip. *Composite Structures*.

Crapps, D. K. (2004). The role of RAM momentum in pile driving. *Geotechnical Special Publication*.

Daniel, I., Hsiao, H., & Cordes, R. (1995). In High Strain Rate Effects on Polymer. *Metal and Ceramic Matrix Composites and Other Advanced Materials, ASME*, *48*, 167–177.

Fam, A., Pando, M., Filz, G., & Rizkalla, S. (2003). Precast piles for route 40 bridge in Virginia using concrete filled FRP tubes. *PCI Journal*.

FDOT. (2019). *FDOT Standard Specifications for Road and Bridge Construction*. Tallahassee,

FL.

FDOT SDG. (2018). *FDOT Structures Design Guidelines*.

Griffiths, L. J., & Martin, D. J. (1974). A study of the dynamic behaviour of a carbon-fibre composite using the split Hopkinson pressure bar. *Journal of Physics D: Applied Physics*.

Holeyman, A. E. (1992). Keynote lecture: Technology of pile dynamic testing. *Proc. 4th Application of Stress Wave Theory to Piles*, 195–215.

Jiang, H., & Chorzepa, M. G. (2015). An effective numerical simulation methodology to predict the impact response of pre-stressed concrete members. *Engineering Failure Analysis*.

Lee, S. L., Chow, Y. K., Karunaratne, G. P., & Wong, K. Y. (1988). Rational wave equation model for pile-driving analysis. *Journal of Geotechnical Engineering*.

Mander, J. B., Priestley, M. J., & Park, R. (1988). Theoretical stress-strain model for confined concrete. *Journal of Structural Engineering (United States)*.

Martinez, S., Nilson, A. H., & O., S. F. (1984). Spirally Reinforced High-Strength Concrete Columns. *ACI Journal Proceedings*, *81*(5).

Melin, L. G., & Asp, L. (1999). Effects of strain rate on transverse tension properties of a carbon/epoxy composite: studied by moiré photography. *Composites Part A: Applied Science and Manufacturing*, *30*(3), 305–316.

Mohamed, H. M., Afifi, M. Z., & Benmokrane, B. (2014). Performance Evaluation of Concrete Columns Reinforced Longitudinally with FRP Bars and Confined with FRP Hoops and Spirals under Axial Load. *Journal of Bridge Engineering*.

Mousa, S., Mohamed, H. M., & Benmokrane, B. (2018). Flexural strength and design analysis of circular reinforced concrete members with glass fiber-reinforced polymer bars and spirals. *ACI Structural Journal*.

Mutalib, A. A., & Hao, H. (2011). Development of P-I diagrams for FRP strengthened RC columns. *International Journal of Impact Engineering*. https://doi.org/10.1016/j.ijimpeng.2010.10.029

Naresh, K., Shankar, K., Rao, B. S., & Velmurugan, R. (2016). Effect of high strain rate on glass/carbon/hybrid fiber reinforced epoxy laminated composites. *Composites Part B: Engineering*.

Ochola, R. O., Marcus, K., Nurick, G. N., & Franz, T. (2004). Mechanical behaviour of glass and carbon fibre reinforced composites at varying strain rates. *Composite Structures*.

Ortlepp, S., & Curbach, M. (2004). Research into high-strength concrete at high rates of loading. *Proceeding of International Symposium on UHPC, Kassel, Germany*, 461–470.

Ou, Y., & Zhu, D. (2015). Tensile behavior of glass fiber reinforced composite at different strain rates and temperatures. *Construction and Building Materials*.

Pando, M., Filz, G., Ealy, C., & Hoppe, E. (2003). Axial and Lateral Load Performance of Two Composite Piles and One Prestressed Concrete Pile. *Transportation Research Record*.

Pantelides, C. P., Gibbons, M. E., & Reaveley, L. D. (2013). Axial Load Behavior of Concrete

Columns Confined with GFRP Spirals. *Journal of Composites for Construction*.

PCI Design Handbook. (1999). *Precast and prestressed concrete*.

Precast/Prestressed Concrete Institute (PCI). (2003). *PCI bridge design manual*. Chicago.

Prince, R. E. (2018). Fiber Reinforced Polymers Characteristics and Behaviors. Retrieved from www.build-on-prince.com/fiber-reinforced-polymers.html

Rajapakse, R. (2008). Pile Design and Construction Rules of Thumb. In *Pile Design and Construction Rules of Thumb*.

Robert, M., & Benmokrane, B. (2013). Combined effects of saline solution and moist concrete on long-term durability of GFRP reinforcing bars. *Construction and Building Materials*.

Roddenberry, M., Mtenga, P., & Joshi, K. (2014). *Investigation of carbon fiber composite cables (CFCC) in prestressed concrete piles.*

Shokrieh, M. M., & Omidi, M. J. (2009a). Compressive response of glass-fiber reinforced polymeric composites to increasing compressive strain rates. *Composite Structures*.

Shokrieh, M. M., & Omidi, M. J. (2009b). Tension behavior of unidirectional glass/epoxy composites under different strain rates. *Composite Structures*.

Smith, E. A. (1960). Pile-driving analysis by the wave equation. *American Society of Civil Engineers Transactions*.

So, A. K. O., & Ng, C. W. W. (2010). Impact compression behaviors of high-capacity long piles. *Canadian Geotechnical Journal*.

Takeda, N., & Wan, L. (1995). In High Strain Rate Effects on Polymer. *Metal and Ceramic Matrix Composites and Other Advanced Materials, ASME*, *48*, 109–133.

Tzeng, J. T., & Abrahamian, A. S. (1996). *Proceedings of the 11th Technical Conference of the American Society for Composites*. 178–188.

Vicaria, J. J. D., Diaz, F. D., Arroyo, M. E., & Paulotto, C. (2014). Analysis of the technical viability of GFRP reinforced precast concrete piles. *16th European Conference on Composite Materials, ECCM 2014*.

Wu, Y., Crawford, J. E., & Magallanes, J. M. (2012). Performance of LS-DYNA Concrete Constitutive Models. *12th International LS-DYNA Users Conference*.